

Article

# Quad-Trapezoidal-Leg Orthoplanar Spring with Piezoelectric Plate for Enhancing the Performances of Vibration Energy Harvester

Yan Liu <sup>1,\*</sup>, Shuting Mo <sup>1</sup>, Siyao Shang <sup>1</sup>, Hai Wang <sup>1</sup>, Peng Wang <sup>2</sup> and Keyuan Yang <sup>3</sup>

<sup>1</sup> Key Laboratory of Electronic Equipment Structure Design, Ministry of Education, Xidian University, Xi'an 710071, China; stmo@stu.xidian.edu.cn (S.M.); syshang@stu.xidian.edu.cn (S.S.); wanghai@mail.xidian.edu.cn (H.W.)

<sup>2</sup> Shaanxi Key Laboratory of Industrial Automation, School of Mechanical Engineering, Shaanxi University of Technology, Hanzhong 723001, China; wangpeng@snut.edu.cn

<sup>3</sup> Academy of Space Information Systems, Xi'an 710100, China; ykymail@126.com

\* Correspondence: liuy@xidian.edu.cn

Received: 14 October 2020; Accepted: 11 November 2020; Published: 13 November 2020



**Abstract:** To validate the potentials of unequal-length section-varied geometry in developing a orthoplanar spring-based piezoelectric vibration energy harvester (PVEH), a modified spring with quad-trapezoidal-leg configuration is designed, analyzed, and fabricated. A basic quad-trapezoidal-leg orthoplanar spring (QTOPS) is theoretically analyzed, and the structural effective stress and eigenfrequency are formulated to determine the main dimension parameters. Then, an improved QTOPS with additional intermediations is constructed and simulated. Prototypes with different leg geometries and mass configurations are fabricated and tested. The results of QTOPS and a conventional rectangular-shaped spring are compared. It is verified that the proposed approach provides the structure with an enlarged effective stress and lower resonant frequency, which makes it more suitable to construct a high-performance PVEH than the orthoplanar spring with equal-length or rectangular legs.

**Keywords:** piezoelectric harvester; orthoplanar spring; trapezoidal leg; vibration energy

## 1. Introduction

Due to the extensive existence of mechanical vibration in ambient environment, the vibration energy harvester (VEH) has been regarded as an important alternative for powering the long-service electronic systems [1,2]. However, the ambient vibration usually features low frequency, varied direction, and weak amplitude, which is a great handicap for harvesting the energy efficiently [3]. Although several energy-harvesting technologies have been utilized, developing a high-performance VEH still faces challenges and attracts great research attention [4].

In particular, research studies regarding the PVEH are actively being conducted, which are targeted at lowering the resonant frequency, broadening the efficient bandwidth, and sensing the weak vibrations. Many excellent solutions have been executed, including multi-mode structure, nonlinearity, frequency up-conversion, etc. [3,5]. The multi-mode approach renders close resonant peaks to PVEH and makes the device advantageous for harvesting the energy in a random environmental vibration [6,7]. The multiple-element array can adapt different target vibrations by combining several basic harvesting units, but the device size is also greatly increased. Then, a multi-mode scheme can also be achieved by using additional masses, by which the structural DOF is increased and peaks close to each other can be realized [8–10]. The nonlinear approach, usually realized by structural nonlinearity and magnetic coupling, works well in broadening the device bandwidth [11,12]. The proposed devices can be monostable, bistable, and tristable, and they are often modeled by the Duffing equation [13–16].

Frequency up-conversion, either in through contact or in a contactless manner, can transmit the low-frequency vibration to the harvesting beam and stimulate it to vibrate at its resonant point, which benefits the device in the operating bandwidth and harvesting efficiency [17–19].

Recently, orthoplanar spring (OPS) is utilized to construct high-performance PVEHs, due to its monolithic planar configuration and capacity of generating normal out-of-plane motion [20]. A series of OPS-based energy harvesters have been reported with multi-mode and nonlinear features [21–23]. The analysis and experimental results showed that favorable multiple nonlinear vibration modes were achieved by the designed compliant orthoplanar springs. Moreover, a quad-leg spring with atypical legs was also studied to show the effect of structural asymmetry [24]. Nevertheless, some supplementary work could be done to further optimize the configuration of OPS. In former literatures, it has been proven that the promotion in effective stress can be fulfilled by introducing unequal-length beams into multi-beam structures [25]. Meanwhile, varying the cross-section of the cantilever has also been utilized to improve the performance of PEVHs [26]. However, most previous works only focus on the symmetrical geometries with equal-length rectangular legs, and the effect of leg shape and length is still not systematically studied.

To validate the potential of unequal-length section-varied geometry in developing OPS-based PVEH and make a contribution to the previous works, this paper focuses on the design and analysis of quad-trapezoidal-leg orthoplanar spring (QTOPS) and explores its application in PVEHs. First, a basic quad-leg structure with trapezoidal legs is formulated to analyze the structural stiffness, stress, and resonant frequency, validating the promotion effect of QTOPS. Then, a modified design for PVEH is constructed and its properties are evaluated via finite element analysis (FEA). After that, a brief description of the device prototype and experimental setup is presented. Finally, characterization experiments are conducted, and conclusions are summarized.

## 2. Design and Analysis

### 2.1. Modeling of the Basic Structure

The basic QTOPS consists of four trapezoidal legs and a central plate. As shown in Figure 1, the legs are arranged around the central plate in a decussate form. A single plan-view for the trapezoidal leg is also defined with proper dimension parameters. The legs can be divided into two groups: two vertical ones with a length of  $L_1$  and two longitudinal ones with a length of  $L_2$ . The QTOPS structure can be regarded as a classical cross-beam-mass pattern, in which the central plate is treated as a rigid mass and supported by the four legs. Based on the displacement of a conventional cross-beam-mass structure and setting  $L_1 = L_2 = L$  for simplicity, the stiffness of QTOPS  $K$  can be correspondingly written as [27]

$$K = \frac{4Et^3a}{AL^3} \quad (1)$$

where  $E$  is the Young's modulus of the material, and  $t$ ,  $a$ , and  $L$  are the thickness, base width, and length of the trapezoidal leg, respectively.  $A$  is a correction factor, which is mainly determined by the ratio of top width  $b$  and base width  $a$ . Combining the formula derived by Sader et al. and the structural response, the factor  $A$  can be approximately expressed as

$$A = \frac{3b/a}{(b/a - 1)^3} \left[ (1 - b/a) - \frac{(1 - b/a)^2}{2b/a} + (b/a) \ln(b/a) \right] \left[ 0.54 + 0.78b/a - 0.28(b/a)^2 \right] \quad (2)$$

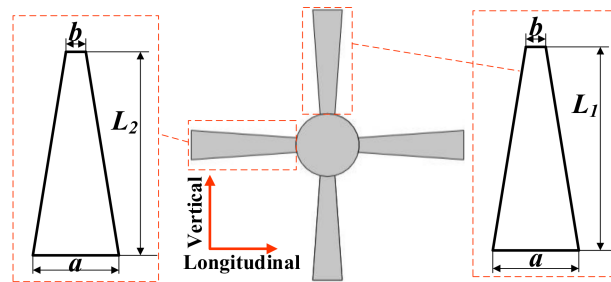


Figure 1. Sketch for the basic quad-trapezoidal-leg orthoplanar spring (QTOPS).

Equation (2) can be divided into two terms:

$$A_1 = \frac{3b/a}{(b/a - 1)^3} \left[ (1 - b/a) - \frac{(1 - b/a)^2}{2b/a} + (b/a) \ln(b/a) \right] \quad (3)$$

$$A_2 = 0.54 + 0.78b/a - 0.28(b/a)^2 \quad (4)$$

$A_1$  is derived from the derived by Sader et al., considering the effect from the shape of the cantilever beam [28,29].  $A_2$  is a supplementary part to accurately represent the cross-beam-mass model of QTOPS, which is obtained by fitting the relationship between the simulated displacement and loaded force of structures with different  $b/a$ . With the obtained function, the structural stiffness can be plot vs.  $b/a$  with  $E = 198$  GPa,  $t = 0.2$  mm,  $a = 15$  mm, and  $L = 50$  mm. Figure 2 shows the calculated stiffness of the basic structure and the results from the force–displacement relationship simulated by finite element analysis (FEA). It can be seen that correction factor  $A$  realizes a favorable precision in bridging the calculated and simulated stiffness. The obtained curve indicates the direct proportion between  $K$  and  $b/a$ .

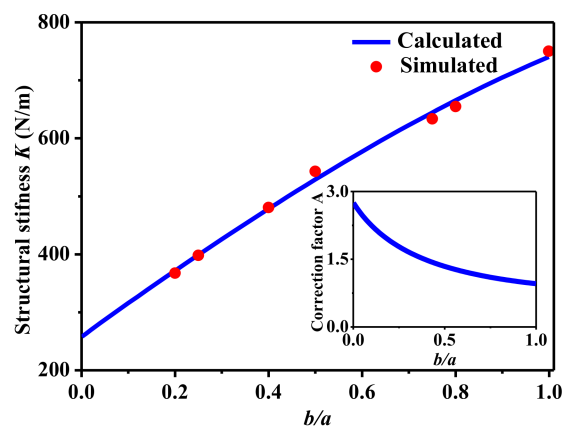


Figure 2. Stiffness and correction factor for the basic structure.

For a certain structure, there are two operating parameters closely related to the performance of PVEH: structural resonant frequency impacts the efficient frequency for PVEH and structural stress under external load determines the energy conversion capability. Sometimes, the frequency and stress can be utilized to evaluate the potential of the proposed structure in constructing a high-performance PVEH [1,30]. With the stiffness function, the eigenfrequency and stress of the basic QTOPS can be easily calculated. A central mass weighing  $25 \times 10^{-3}$  kg is added to the model, and an  $10 \text{ m/s}^2$  acceleration is applied. Figure 3 plots the results for structural eigenfrequency and the maximum stress of a leg under different combinations of leg length ratio and  $b/a$ . In the analysis, the length of two vertical legs ( $L_1$ ) is set as 50 mm and the two longitudinal legs are shortened to achieve different length ratios ( $L_2/L_1$ ). A lower frequency can be observed under a larger  $L_2/L_1$  ratio and smaller  $b/a$ , and a

larger stress can be obtained under a smaller  $L_2/L_1$  and  $b/a$ . The results verify the enhancing capacity of unequal-length configuration and a trapezoidal-shaped leg. Based on the results, the basic structure with the combination of  $b/a = 0.5$  and  $L_2/L_1 = 0.8$  is chosen as the fundamental frame to construct the desired PVEH.

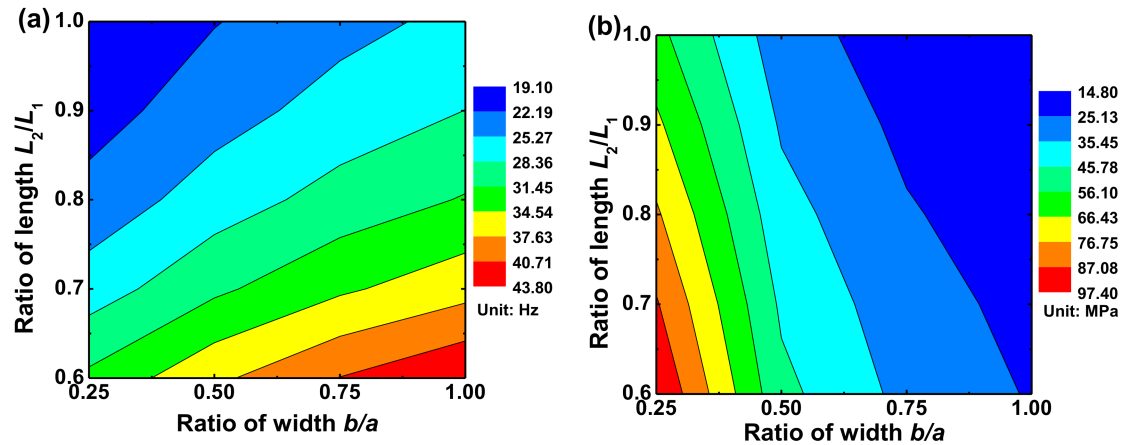


Figure 3. Calculated eigenfrequency (a) and maximum stress (b) of the basic QTOPS.

### 2.2. Construction of the PVEH

To fully exploit the features of the basic structure, an improved geometry with four additional intermediations is proposed to construct the desired PVEH. Figure 4 depicts the proposed QTOPS-based schemes for PVEH and their nomenclature. Benefiting from the introduction of intermediations, more than one mass can be easily placed in the device, including the  $M_c$  (center),  $M_1/M_2$  (intermediation at short leg), and  $M_3/M_4$  (intermediation at long leg). In the proposed PVEH schemes, the piezoelectric plates could be arranged at the ends of legs for performance comparison, as shown in Figure 4. When put into practical applications, the PVEH will be mounted onto the targets by fixing the ends indicated by the red triangles, which is also utilized as a constraint condition in the following simulation and prototype characterization.

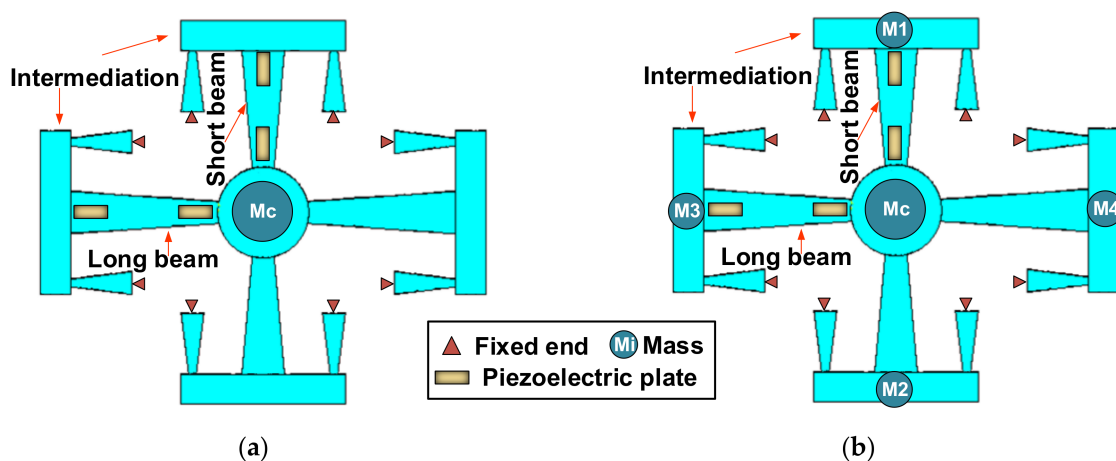


Figure 4. The energy harvester based on the QTOPS with Case 1 (a) and Case 2 (b) configurations.

After introducing the intermediations and necessary ancillaries, the structural complexity is significantly increased, making it difficult to theoretically formulate the resonant frequency and stress of the proposed scheme. Herein, the finite element analysis (FEA), an effective and widely used method in structural engineering, is employed to analyze the target features [31,32]. In the analysis, two different combinations of mass (Case 1: only  $M_c$  and Case 2:  $M_c + M_1-M_4$ ) are used. The finite

element models of the proposed QTOPS and conventional quad-rectangular-leg OPS (QROPS) were developed using commercial package ANSYS 14.5 (ANSYS Inc., Canonsburg, PA, USA). The whole structures were meshed with 3D SOLID95 elements, in which every element was defined by 20 nodes with three degrees of freedom per node. The whole structures of Case 1-based and Case 2-based QTOPS were discretized with 55,018 and 47,214 elements respectively; the values were 45,361 and 38,541 for Case 1-based and Case 2-based QROPS. In all simulations, the constraint condition was loaded by constraining all the freedoms of fixed ends indicated by the red triangles in Figure 4. Firstly, static analysis is conducted to study the stress distribution along the legs, and the results can help to further refine the positions of piezoelectric plates. Then, modal analysis is conducted to evaluate the resonant frequency. The parameters for simulation are shown in Table 1. A  $10 \text{ m/s}^2$  acceleration is loaded, and the weight of masses is settled as  $M_c = 25 \times 10^{-3} \text{ kg}$ ,  $M_1 = M_2 = M_3 = M_4 = 10 \times 10^{-3} \text{ kg}$ .

**Table 1.** Parameters for finite element analysis (FEA) simulation.

Material Parameters			Dimension				
Young Modulus (GPa)	Poisson's Ratio	Density ( $\text{kg/m}^3$ )	Length of Long Leg (mm)	Base Width (mm)	Thickness (mm)	$L_2/L_1$	$b/a$
198	0.3	7810	50	15	0.2	0.8	0.5

Figure 5a presents the stress distribution in the proposed QTOPS under Case 1. For easy description, the leg end connecting with the central plate is denominated as the top end, and the other one is named as the base end. It can be seen that more considerable stresses develop at the top end of legs. More clarity for the stress distribution is plotted in Figure 5b by mapping the normal stress onto the preset paths, which are coincident with the centerline of their corresponding legs (also shown in Figure 5a). In Figure 5b, the sharp variation of every curve presents the stress decrease in the thick plate region, which has the same length in every curve but is modulated by the different scales for long and short legs. Compared with conventional QROPS, the stress in the top end of the short and long leg is lifted to 152.8% and 150.4%, respectively. Meanwhile, the stress distribution curves also verify the enhancing effect of the proposed unequal-length configuration. The maximum stress of the short leg in QTOPS is 41.8% larger than that of the long leg. Based on the results, the piezoelectric plates should cover the top end of the short leg to make better use of the energy seized by QTOPS.

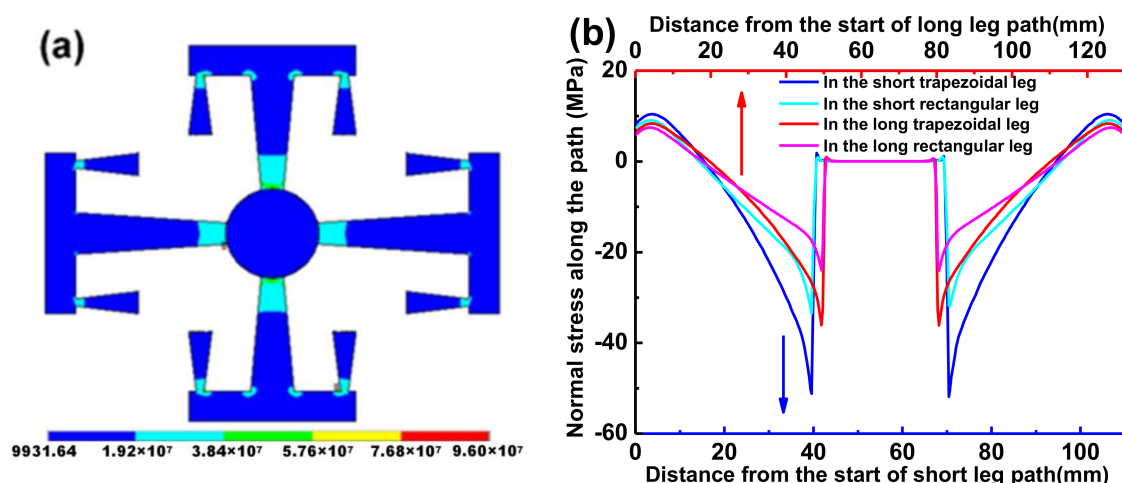


**Figure 5.** Stress distribution for Case 1: (a) von Mises stress and (b) normal stress along the leg paths.

The stress results of Case 2-based QTOPS are shown in Figure 6. Similarly, the stress concentrates more at the top end of the legs, and the trapezoidal unequal scheme also promotes the stress values. Compared with QROPS, the maximum stress in the short and long trapezoidal legs is lifted to 167.5% and 165.3%, respectively. Meanwhile, the short leg in Case 2 also features a stress that is 1.36 times the

value of that in the long leg. These results under Case 2 further validate the superiority of QTOPS in promoting the effective stress for harvesting the vibration efficiently.

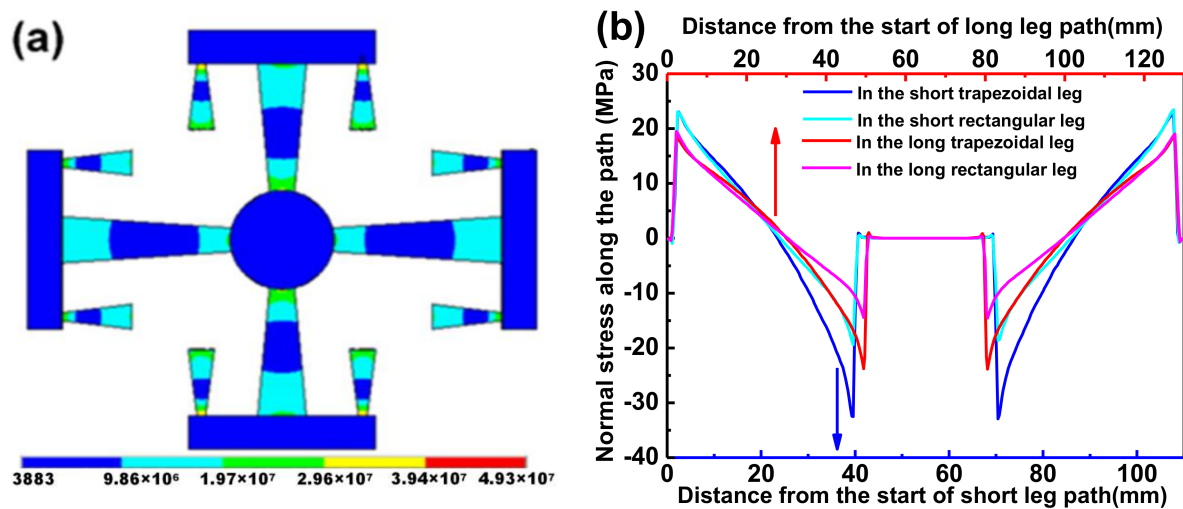


Figure 6. Stress distribution for Case 2: (a) von Mises stress and (b) normal stress along the leg paths.

Modal analysis is also conducted to evaluate the dynamic response of the proposed QTOPS-based PVEH. When only utilizing the central mass (namely Case 1), the OPS presents just one mode below 50 Hz (17.6 Hz), as shown in Figure 7. When adding additional four intermediate masses (Case 2), five modes below 50 Hz (20.7, 33.9, 34.2, 34.6, and 36.4 Hz) can be achieved. The introduction of intermediate mass produces a potential in realizing a multi-mode vibration energy harvester. Meanwhile, the trapezoidal scheme exhibits lower resonant frequencies than the rectangular scheme in both Case 1 and Case 2, further distinguishing the superiority of QTOPS-based PVEH.

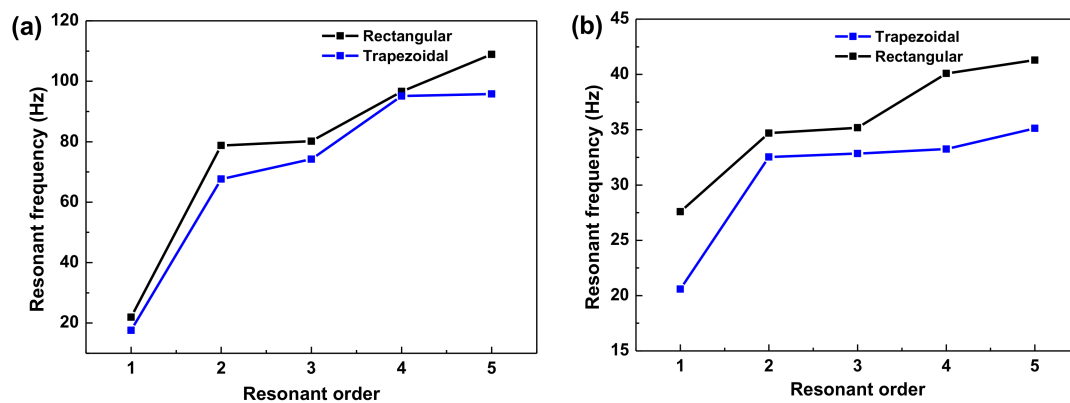


Figure 7. Resonant frequency of Case 1-based (a) and Case 2-based (b) devices.

### 3. Prototypes and Experiments

To verify the designed potentials of proposed QTOPS in PVEH, several prototypes are fabricated with a 0.2 mm-thick spring steel (Metal grade 65 Mn) film, whose parameters are the same as the values in Table 1. The long leg is set at 50 mm for length, 15 mm for base width, and 7.5 mm for top width. Correspondingly, the short leg is set at 40 mm for length, 15 mm for base width, and 7.5 mm for top width. The length ratio between the short and long leg is 0.8, and the width ratio between the base and top is 0.5, which is consistent with the design parameters. The masses are added by attaching proper iron blocks in the central plate and intermediations, and piezoelectric plates made of lead zirconate titanate ceramics (Type: PZT-5A) [4] with the dimensions of 7 mm × 15 mm × 0.23 mm (width × length × thickness) are adhered onto the top end of the legs. An additional prototype with QROPS is also

built for comparison, whose leg lengths are the same as with the trapezoidal approach, but the width is kept as 15 mm.

An experimental setup, as shown in Figure 8, is built to test the prototypes. Stimulating vibration is produced by a shaker system, in which the function generator (SDG1020, SIGLENT, Shenzhen, China) provides sinusoidal voltage with varied frequency and the signal is amplified by the power amplifier (SD1492A, BDHSD, Qinhuangdao, China) to excite the shaker (SD1482A, BDHSD, Qinhuangdao, China). An oscilloscope (GDS-1072B, GWINSTEK, Suzhou, China) is utilized to measure the generated voltage by PVEH prototypes and monitor the output of the accelerometer (CA-YD-180, BDHSD, Qinhuangdao, China). The current source (SD14T03, BDHSD, Qinhuangdao, China) is used to transform the output of the accelerometer into voltage form.

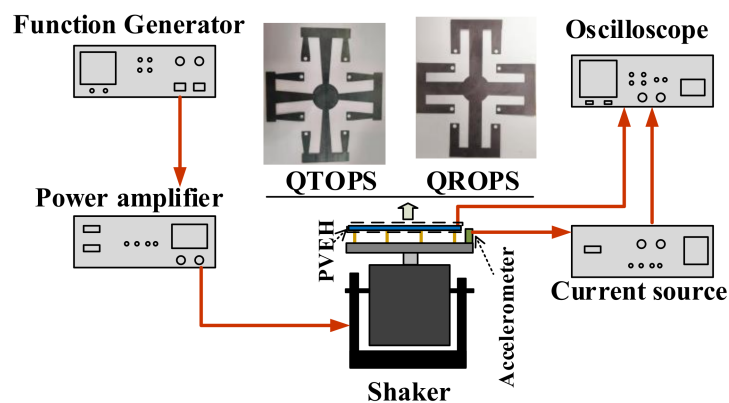


Figure 8. Experimental setup.

## 4. Results

In this section, we present the voltage and power outputs of the QTOPS-based PVEH. An additional QROPS-based prototype is also measured as a contrast. The characteristics of devices under different mass locations (Case 1 and Case 2) are tested, and the target vibration is imitated by a sinusoidal acceleration with an amplitude of  $10 \text{ m/s}^2$  and different frequencies. In the experiments, the prototypes are firstly stimulated by the loaded vibrations to obtain their working frequencies (resonance frequencies) by testing their generated voltages at different frequencies. Then, the power tests are conducted by recording the voltage over the loaded resistors when the devices are stimulated at their working frequencies. All the experiments are conducted at room temperature of  $25 \text{ }^\circ\text{C}$  and a humidity of 55% RH.

### 4.1. Results for Case 1-Based Prototypes

First, the open-circuit output voltage of Case 1 configurations is tested, and the voltage–frequency (V-f) curve is shown in Figure 9a. The curves with same color indicate the results of the same prototype, but the piezoelectric plates are respectively located at the short leg (solid markers) and long leg (hollow markers). The QTOPS resonates at 16.4 Hz with corresponding peak voltages of 13.45 V and 9.25 V for the short and long leg, respectively. Meanwhile, the QROPS has a resonant frequency of 19.2 Hz, and its peak voltages are 8.70 V and 6.42 V for the short and long leg, respectively. Compared with QROPS, the utilization of the trapezoidal leg provides a  $1.55\times$  increase to the generated voltage and a decline of 14.6% to the resonant frequency. Meanwhile, the short leg features a higher voltage in both QTOPS and QROPS, and the promotion can be up to 145.4%. However, there is only one resonant peak in the range of 0–50 Hz for both QTOPS and QROPS devices.

Figure 9b presents the power–load resistance curve of these devices at their resonance frequencies of 16.4 and 19.2 Hz, respectively. The best matching resistance for QTOPS-based PVEH is about 296 k $\Omega$ , and the corresponding output power is 192.9 and 84.9  $\mu\text{W}$  for short and long legs; the values of QROPS-based PVEH are about 256 k $\Omega$  for optimized resistance, and 89.1 and 42.7  $\mu\text{W}$  for output

power in short and long legs. Obviously, the short leg in QTOPS-based PVEH generates a larger output power.

Generally, both the trapezoidal leg and unequal-length approach can achieve an improvement in the performance of the PVEH, which is accordant with the design results and verifies the validity of the proposed scheme.

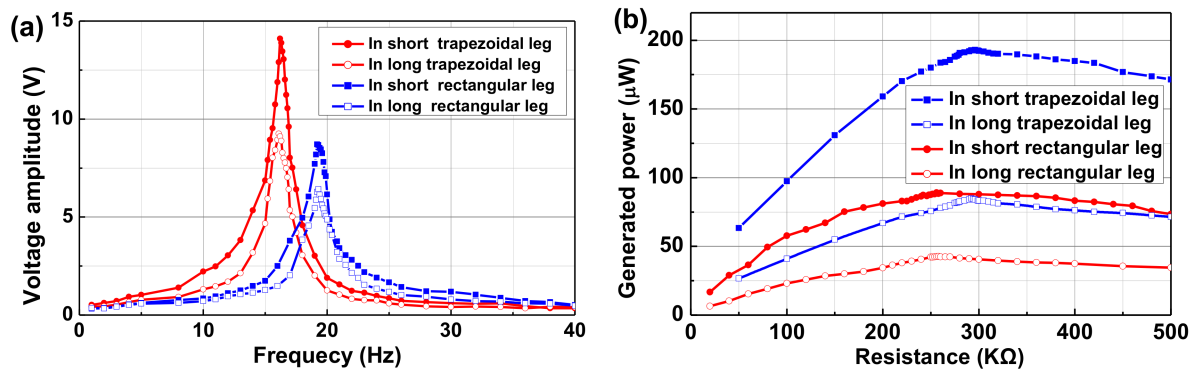


**Figure 9.** Experimental results for Case 1-based prototypes with the different locations for the piezoelectric plate: (a) voltage vs. frequency and (b) power vs. load resistance.

#### 4.2. Results for Case 2-Based Prototypes

The V-f curves of Case 2-based prototypes are shown in Figure 10a. Herein, the QTOPS obtains three resonant peaks at 18.7, 30.5, and 33 Hz in the frequency range of 0–50 Hz with voltages of 7.32, 2.58, and 1.42 V in the short leg and 5.12, 1.25, and 0.943 V in the long leg. Meanwhile, the QROPS also generates three peaks in the range of 0–50 Hz, but its voltage value is at most 61.9% of QTOPS and the frequency is at least 8.85% higher.

The output power of the first three peaks in the V-f curves is also studied. Figure 10b shows the maximum power in the short leg of QTOPS and QROPS under respective optimized resistances. The first peak has the largest power, and the value exhibits a downtrend in the following peaks. Evidently, the QTOPS-based PVEH also possesses a better harvesting efficiency than the QROPS-based one. As for the power long legs, a similar circumstance can be seen, but the values are much smaller than those of short legs.

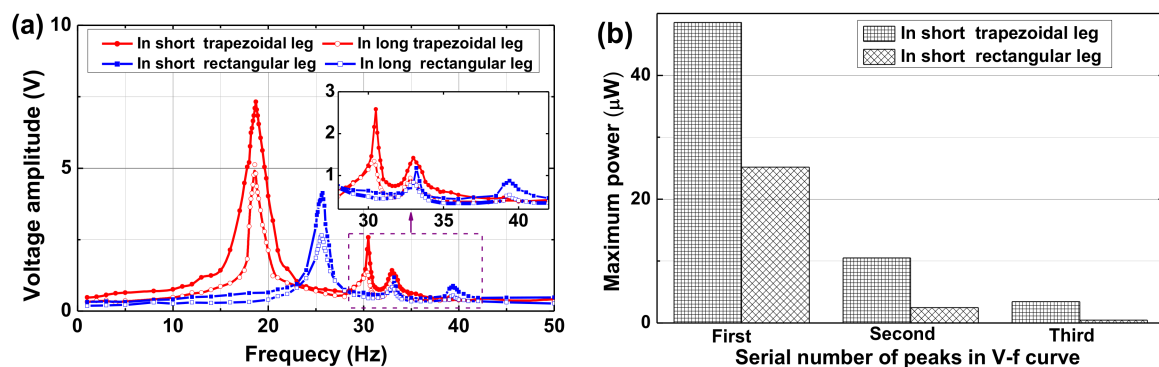


**Figure 10.** Experimental results for Case 2-based prototypes with the different locations for the piezoelectric plate: (a) voltage vs. frequency and (b) maximum power at the peaks of V-f curve.

#### 4.3. Discussion

Based on the obtained experimental values, a brief discussion about the validation of the structural design and simulation results are conducted. As mentioned above, the applied stress determined the generated voltage of the piezoelectric plates. Therefore, comparisons between the simulated

results of maximum stress and measured results of maximum voltage are conducted for both the Case 1-based and Case 2-based prototypes. The compared results are shown in Table 2. In the comparisons, the value ratios of maximum stress in the legs with different shapes and lengths are calculated to compared with the corresponding value ratios of maximum voltage. It can be seen that the value ratios based on experimental results are well accorded with the ratios based on simulated results, indicating the feasibility of analyzing the PVEH performance with the help of simulated stress. Moreover, the performance enhancement realized by using QTOPS-based scheme is also verified by both simulations and experiments.

**Table 2.** Comparison between the simulated and measured results.

Source of Compared Values		$N_1$ <sup>a</sup>	$N_2$ <sup>a</sup>	Deviation = $(N_2 - N_1)/N_2 \times 100\%$
Case 1	Situation 1 <sup>b</sup>	1.528	1.55	1.44%
	Situation 2 <sup>b</sup>	1.418	1.454	2.48%
Case 2	Situation 1 <sup>b</sup>	1.675	1.615	−3.71%
	Situation 2 <sup>b</sup>	1.36	1.429	4.83%

<sup>a</sup>  $N_1$  is the value ratio of simulated maximum stress,  $N_2$  is the value ratio of measured maximum voltage; <sup>b</sup> Situation 1 is Short trapezoidal leg vs. short rectangular leg, Situation 2 is Short trapezoidal leg vs. long trapezoidal leg.

## 5. Conclusions

In this paper, a piezoelectric vibration energy harvester based on improved orthoplanar spring is designed, fabricated, and tested. Four unequal-length trapezoidal legs are adopted to construct the basic structure and theoretically validate the structural potential in lifting the device performance. Then, a modified geometry is proposed for building the final PVEH, whose properties are verified by finite element analysis. The utilization of a trapezoidal leg increases the effective stress and declines the structural resonant frequency, and the combination of short and long legs further promotes the harvesting capacity. The experimental results show that the short leg in QTOPS-based PVEH can generate a peak open-circuit output voltage of 13.45 V with the maximum power of 192.9  $\mu$ W when the device is excited by a 10 m/s<sup>2</sup> sinusoidal acceleration. The power value is 2.27 times that of the long leg in QTOPS and 2.16 times that of the short leg in QROPS. Meanwhile, the resonance frequency is decreased by 14.6%, showing a better capacity of adapting to the low-ambient vibrations. The multi-mode property is also realized by adding more masses into the structure, and the enhancing effect of the unequal-length trapezoidal configuration is also perceptible. The superiority of using QTOPS has been verified by both simulated and experimental results, but the device commercialization is still limited by the generated power and structural compactness. Further structural optimization and miniaturization is still needed in the future work to promote the device characteristics.

**Author Contributions:** Conceptualization, Y.L. and S.M.; methodology, Y.L. and S.S.; software, H.W. and K.Y.; validation, Y.L. and P.W.; writing—original draft preparation, Y.L. and P.W.; writing—review and editing, Y.L. and S.S. All authors have read and agreed to the published version of the manuscript.

**Funding:** This research was funded by Natural Science Basic Research Program of Shaanxi, grant numbers 2020JQ-309 and 2020JQ-872.

**Conflicts of Interest:** The authors declare no conflict of interest.

## References

1. Toprak, A.; Tigli, O. Piezoelectric energy harvesting: State-of-the-art and challenges. *Appl. Phys. Rev.* **2014**, *1*, 031104. [[CrossRef](#)]
2. Liu, Y.; Wang, H.; Zhao, W.; Zhang, M.; Qin, H.; Xie, Y. Flexible, stretchable sensors for wearable health monitoring: Sensing mechanisms, materials, fabrication strategies and features. *Sensors* **2018**, *18*, 645. [[CrossRef](#)] [[PubMed](#)]

3. Yildirim, T.; Ghayesh, M.H.; Li, W.; Alici, G. A review on performance enhancement techniques for ambient vibration energy harvesters. *Renew. Sustain. Energy Rev.* **2017**, *71*, 435–449. [[CrossRef](#)]
4. Yang, Z.; Zhou, S.; Zu, J.; Inman, D. High-performance piezoelectric energy harvesters and their applications. *Joule* **2018**, *2*, 642–697. [[CrossRef](#)]
5. Tran, N.; Ghayesh, M.H.; Arjomandi, M. Ambient vibration energy harvesters: A review on nonlinear techniques for performance enhancement. *Int. J. Eng. Sci.* **2018**, *127*, 162–185. [[CrossRef](#)]
6. Luo, C.; Xu, H.; Wang, Y.; Li, P.; Hu, J.; Zhang, W. Unsymmetrical, interdigital vibration energy harvester: Bandwidth adjustment based on mode separation technique. *Sens. Actuators A Phys.* **2017**, *257*, 30–37. [[CrossRef](#)]
7. Deng, H.; Du, Y.; Wang, Z.; Zhang, J.; Ma, M.; Zhong, X. A multimodal and multidirectional vibrational energy harvester using a double-branched beam. *Appl. Phys. Lett.* **2018**, *112*, 213901. [[CrossRef](#)]
8. Aldraihem, O.; Baz, A. Energy harvester with a dynamic magnifier. *J. Intell. Mater. Syst. Struct.* **2011**, *22*, 521–530. [[CrossRef](#)]
9. Li, X.; Upadrashta, D.; Yu, K.; Yang, Y. Analytical modeling and validation of multi-mode piezoelectric energy harvester. *Mech. Syst. Signal Process.* **2019**, *124*, 613–631. [[CrossRef](#)]
10. Tang, L.; Yang, Y. A multiple-degree-of-freedom piezoelectric energy harvesting model. *J. Intell. Mater. Syst. Struct.* **2012**, *23*, 1631–1647. [[CrossRef](#)]
11. Daqaq, M.F.; Masana, R.; Erturk, A.; Dane Quinn, D. On the role of nonlinearities in vibratory energy harvesting: A critical review and discussion. *Appl. Mech. Rev.* **2014**, *66*, 040801. [[CrossRef](#)]
12. Pellegrini, S.P.; Tolou, N.; Schenk, M.; Herder, J.L. Bistable vibration energy harvesters: A review. *J. Intell. Mater. Syst. Struct.* **2012**, *24*, 1303–1312. [[CrossRef](#)]
13. Andò, B.; Baglio, S.; Bulsara, A.R.; Marletta, V. A bistable buckled beam based approach for vibrational energy harvesting. *Sens. Actuators A Phys.* **2014**, *211*, 153–161. [[CrossRef](#)]
14. Fan, K.; Tan, Q.; Liu, H.; Zhang, Y.; Cai, M. Improved energy harvesting from low-frequency small vibrations through a monostable piezoelectric energy harvester. *Mech. Syst. Signal Process.* **2019**, *117*, 594–608. [[CrossRef](#)]
15. Shan, G.; Wang, D.F.; Song, J.; Fu, Y.; Yang, X. A spring-assisted adaptive bistable energy harvester for high output in low-excitation. *Microsyst. Technol.* **2018**, *24*, 3579–3588. [[CrossRef](#)]
16. Zhou, S.; Cao, J.; Litak, G.; Lin, J. Numerical analysis and experimental verification of broadband tristable energy harvesters. *tm-Tech. Messen* **2018**, *85*, 521–532. [[CrossRef](#)]
17. Deng, H.; Wang, Z.; Du, Y.; Zhang, J.; Ma, M.; Zhong, X. A seesaw-type approach for enhancing nonlinear energy harvesting. *Appl. Phys. Lett.* **2018**, *112*, 213902. [[CrossRef](#)]
18. Kwon, D.-S.; Ko, H.-J.; Kim, M.-O.; Oh, Y.; Sim, J.; Lee, K.; Cho, K.-H.; Kim, J. Piezoelectric energy harvester converting strain energy into kinetic energy for extremely low frequency operation. *Appl. Phys. Lett.* **2014**, *104*, 113904. [[CrossRef](#)]
19. Kathpalia, B.; Tan, D.; Stern, I.; Erturk, A. An experimentally validated model for geometrically nonlinear plucking-based frequency up-conversion in energy harvesting. *Smart Mater. Struct.* **2018**, *27*, 015024. [[CrossRef](#)]
20. Parise, J.J.; Howell, L.L.; Magleby, S.P. Ortho-planar linear-motion springs. *Mech. Mach. Theory* **2001**, *36*, 1281–1299. [[CrossRef](#)]
21. Nabavi, S.; Zhang, L. Nonlinear multi-mode wideband piezoelectric mems vibration energy harvester. *IEEE Sens. J.* **2019**, *19*, 4837–4848. [[CrossRef](#)]
22. Dhote, S.; Yang, Z.; Zu, J. Modeling and experimental parametric study of a tri-leg compliant orthoplanar spring based multi-mode piezoelectric energy harvester. *Mech. Syst. Signal Process.* **2018**, *98*, 268–280. [[CrossRef](#)]
23. Dhote, S.; Zu, J.; Zhu, Y. A nonlinear multi-mode wideband piezoelectric vibration-based energy harvester using compliant orthoplanar spring. *Appl. Phys. Lett.* **2015**, *106*, 163903. [[CrossRef](#)]
24. Dhote, S.; Li, H.; Yang, Z. Multi-frequency responses of compliant orthoplanar spring designs for widening the bandwidth of piezoelectric energy harvesters. *Int. J. Mech. Sci.* **2019**, *157–158*, 684–691. [[CrossRef](#)]
25. Wang, P.; Zhao, Y.; Tian, B.; Liu, Y.; Wang, Z.; Li, C.; Zhao, Y. A piezoresistive micro-accelerometer with high frequency response and low transverse effect. *Meas. Sci. Technol.* **2017**, *28*, 015103. [[CrossRef](#)]
26. Savarimuthu, K.; Sankararajan, R. Design and analysis of cantilever based piezoelectric vibration energy harvester. *Circuit World* **2018**, *44*, 78–86. [[CrossRef](#)]

27. Bao, M.-H. *Micro Mechanical Transducers: Pressure Sensors, Accelerometers and Gyroscopes*; Elsevier: Amsterdam, The Netherlands, 2000.
28. Sader, J.E.; White, L. Theoretical analysis of the static deflection of plates for atomic force microscope applications. *J. Appl. Phys.* **1993**, *74*, 1–9. [[CrossRef](#)]
29. Slattery, A.D.; Blanch, A.J.; Shearer, C.J.; Stapleton, A.J.; Goreham, R.V.; Harmer, S.L.; Quinton, J.S.; Gibson, C.T. Characterisation of the material and mechanical properties of atomic force microscope cantilevers with a plan-view trapezoidal geometry. *Appl. Sci.* **2019**, *9*, 2604. [[CrossRef](#)]
30. van Kempen, R.B.; Herder, J.L.; Tolou, N. A Strain Distribution Based Classification of Ortho-Planar Springs: An Outlook to Piezoelectric Applications. In *ASME 2016 International Design Engineering Technical Conferences and Computers and Information in Engineering Conference*; ASME: Charlotte, NC, USA, 2016; Volume 4, p. V004T008A013.
31. Wang, L.; Ding, J.; Jiang, Z.; Luo, G.; Zhao, L.; Lu, D.; Yang, X.; Ryutaro, M. A packaged piezoelectric vibration energy harvester with high power and broadband characteristics. *Sens. Actuators A Phys.* **2019**, *295*, 629–636. [[CrossRef](#)]
32. Wang, L.; Zhao, L.; Jiang, Z.; Luo, G.; Yang, P.; Han, X.; Li, X.; Maeda, R. High accuracy comsol simulation method of bimorph cantilever for piezoelectric vibration energy harvesting. *AIP Adv.* **2019**, *9*, 095067. [[CrossRef](#)]

**Publisher’s Note:** MDPI stays neutral with regard to jurisdictional claims in published maps and institutional affiliations.



© 2020 by the authors. Licensee MDPI, Basel, Switzerland. This article is an open access article distributed under the terms and conditions of the Creative Commons Attribution (CC BY) license (<http://creativecommons.org/licenses/by/4.0/>).